New Fuel Cell Tubular Architecture and the Effect of Electrokinetic Flows in its Performance

L.A.W. Bambace[1], F.M. Ramos[2], H.F. Villanova[1], A.J. Alvim de Castro[3], R.C. Favalli[3]

[1] Space Mechanics and Control Division, National Institute for Space Research -INPE, São José dos Campos, São Paulo, BRAZIL. Tel +55 12 3945-6154 bambace@dem.inpe.br hnova@dem.inpe.br
[2] International Affairs Adviser, National Institute for Space Research -INPE, São José dos Campos, São Paulo, BRAZIL. Tel +55 12 3945-6024 fernando@lac.inpe.br
[3] Nuclear Engineering Center, Instituto de Pesquisas Energéticas e Nucleares-IPEN/CNEN-SP São Paulo, São Paulo, BRAZIL. Tel +55 11 3133-9452

1 Abstract

This papers introduces a brand new family of fuel cell architectures based on micrometer diameters tubes with walls of nanometer scale pores and high void fraction gathered in nonwoven arrangements, and discusses the role of: transport phenomena, electrokinetic flows (EKF), gas-liquid interface area, convective mix, and the electrical boundary layer (EBL) in these fuel cells performance. Its also discuss the introduces the concept of hidden hydrogen catalyst, possible due to the large interface area.

2 Introduction

Performances of all low temperature fuel cell are limited by transport phenomena. According to flooded models, common a plane gas-liquid interface PEM has its peak power O_2 diffusion entry limited to a few nanometers [1]. The use of test probes in such PEM cathodes proved that only a minor part of the catalyst layer is truly active [2]. Besides the low O_2 solubility in alkaline liquids [3], ionic current also limited Adams-Watson-Bacon fuel cell, one of the cells with better breathing, as its electrodes had a low electrolyte volume fraction and high tortuosities [4]. Ledoux et al. [5], Bambace et al. [6-13] and Tenninson et al. [14] tried to enhance cell transport phenomena, respectively with carbon fiber with covers of entangled carbon nanotubes, and tubular electrodes set ups with external and internal air flow. MEMS and micro-fluidic fuel cells are also in the literature [15,16]. External air tubular setups have high breathing areas and EKF effects in ionic current transport. In an electroosmotic flow (EOF) chemical reactions control EBL charge levels as: dissociation of PEM membranes sulfonic groups or glass silanol. Capacitive effects prevail in electrocapillary systems (metal-bath interfaces). Top EKF speeds in 1-10 μm metal ducts can´t be found with simple capillary and pressure drop forces balances: the flow itself reduces its force drivers. Knudsen numbers based on EBL thickness in the 0.03-0.15 range, point an slip flow possibility. Mobility and surface diffusion of adsorbed ions are known to reduce roughness in electroplating parts. So, the non-slip condition is not valid, and EKF models needs experimental parameters. The convection inside the not neutral EBL helps ionic current transport, reducing its dissipation, and is predicted by the Onsager´s principle [17] once despite of flow dissipation the overall losses are reduced. The anodes may operate with ionomer in the μm tubes wall either with exposed or hidden catalyst. In H_2 hidden catalyst system, CO is blocked by the external cover, and O_2 anode poisoning controlled by the H_2 flow in the structure.

3 Theoretical Model

Static electrocapillary was described in the 19th century by Lippmann, who noticed that mercury surface tension had a parabolic profile with a maximum for uncharged liquid. For molecules with dipoles in the electrolyte, the surface tension σ is given in Grahame model by:

$$\sigma = \sigma_o - 0{,}5(C/A)\Delta U^2 + \Sigma_i\{B_i \ln(1+b_k[a_i])\} \qquad (1)$$

where σ_o is the uncharged pure liquid surface tension, C the electrical capacity, A the area, U the electrical potential, $B_i \in R$, an influence coefficient, $[a_i]$ the concentration of dissolved ion i, and b_k are constants. The energy is the dσ/dx integral over a surface, so capillary force in any channel of fixed perimeter p, with tip σ values being σ_1 and σ_2 and $p(\sigma_1-\sigma_2)$. For a tube of diameter d, length L, and fluid dynamic viscosity μ, the force balance is given by the flow speed of $(\sigma_1-\sigma_2)L^{-1}\mu^{-1}d/8$ if standard speed profiles are used. Large tubes don´t show such speeds no matter what causes the changes of σ. An EBL of thickness x_o has a non-diffuse part of thickness x_2 (nEBL) of organized layers over adsorbed anions and molecules where dipoles forces prevail. It also has a diffuse sublayer (dEBL) that obeys an one-dimensional Gauss equation, as Poisson-Boltzmann (PB) so for φ=UF/(RT),and q=1:

$$\nabla^2\varphi = \varepsilon^{-1}\gamma_e = -K^2 \Sigma\, n_i\, n_o^{-1} \exp(-q\, z_i\varphi) \qquad (2)$$

where the potential reference is set far away from the surface, a place with ion concentration a_∞, F is the Faraday constant, R the universal gas constant, T the absolute temperature, for y a coordinate parallel to the surface K is $[2z_i^2F^2a_\infty(y)]^{1/2}[\varepsilon RT]^{-1/2}$, z_i is the number of charges of ions, γ_e the volume charge density, ε the media dielectric constant. Replacing Boltzmann distribution other equations arise [18-19], generally written in similar form with other q and K, at least as an approximation. The solution of equation (2) is often written for constant z_i=z in implicit form:

$$\tanh(0.25\varphi)=\tanh(0.25\varphi_2(y))\exp(-K(x-x_2)) \qquad (3)$$

where $\varphi_2(y)$ is the dimensionless potential at x_2, and x the distance from the surface. Equation (3) may be rewritten, with $\delta=zF/(RT)$ and $\zeta(y)=\varphi_2(y)\delta^{-1}$ in explicit form as:

$$G(x,y)=\tanh(0.25\,\delta\zeta(y))\exp(-K(x-x_2)) \qquad (4.a)$$
$$U(x,y)=2\delta^{-1}\ln\{1+G(x,y)\}-2\delta^{-1}\ln\{1-G(x,y)\} \qquad (4.b)$$

Unit area capacities c ≡ (C/A) may be split in diffuse and non-diffuse parts, $c_m=(x_o-x_2)/\varepsilon$ and $c_2=x_2/\varepsilon$. PB fails to model cathode and anode c differences. In the EBL there is an electrical field $\mathbf{E}_o$ in the direction $\hat{\mathbf{e}}_y$ and a much stronger field $\mathbf{E}_x$ in the direction $\hat{\mathbf{e}}_x$ normal to the metal surface, where charge density ν is $[8RT\varepsilon a_\infty]^{1/2}\sinh(0.5\,\delta\zeta)$ in PB. U and ionic resistivity ρ obeys the Laplace Equation, thus for E the electrical field:

$$c^{-1}=\{\varepsilon^{-1}[\cosh(\delta\zeta(y)/2)]^{-1}K^{-1}+\varepsilon^{-1}x_2\}=c_2^{-1}+c_m^{-1} \qquad (5)$$

$$\mathbf{E} = -\nabla U \qquad (6)$$
$$\nabla\rho^{-1}\nabla U= 0 \qquad (7)$$

As the layer is thin γ_e~ε d^2U/dx^2.Continuity, Navier Stokes and species concentration equations are:

$$\nabla^o\mathbf{u} = \nabla^o(u_x\,\hat{\mathbf{e}}_x+ u_y\,\hat{\mathbf{e}}_y) = 0 \qquad (8)$$
$$\omega\, u_i\, d\mathbf{u}/dx_i = -\nabla P + \mu\nabla^2\mathbf{u} + \gamma_e\,\mathbf{E} \qquad (9)$$
$$-D_i\nabla^2a_i+\mathbf{m}_i\nabla^o(\mathbf{E}\, a_i)+\nabla^o(\mathbf{u}\, a_i)+\chi_{qi}-\chi_{qo}= 0 \qquad (10)$$

where ω is the fluid density, a_i species i concentration, χ_{qi} and χ_{qo} chemical conversion rates, $\mathbf{m_i}$ ionic mobility, D_i diffusion coefficient. EBL speed component normal to a solid is negligible, and, 2 nm<x_o<5 nm, to P_∞ the far away pressure, pressure is $P(x,y)=P_\infty(y)+\varepsilon\,(dU/dx)^2/2$. Due to adsorbed ions surface diffusion and mobility of, and a possible slipping boundary condition, a tube fluid velocity **u** may be split in 4 wall parallel parts: a nEBL slip v_{OHP} at x_2, $u_p=(\zeta-U)\varepsilon\mathbf{E}_o\mu^{-1}$, $u_m=U_m(r^2/R^2)$, and v_p; and **s** normal to wall. G≡0 out of EBL, dU/dx=0 if U=0, so:

$$\begin{aligned}&[\varepsilon d^2U/dx^2\mathbf{E}_o-\mu d^2u_p/dx^2]+\\ &+[dP/dy+4\mu U_mR^{-2}+\Delta P_a+\omega u du/dy+\omega s du/dx]-\\ &-[\mu d^2v_p/dx^2-\varepsilon dU/dx\, d^2U/dxdy-\varepsilon dU/dy\, d^2U/dx^2]\end{aligned} \qquad (11)$$

Setting the 1st line of equation (11) to zero, one gets the classical EOF equation, solved by the u_p, the 2nd line governs flow out of the EBL, and is solved by u_m if **s**≡0. The 3rd bracket refers to the electrocapillary extra component v_p, function of electrical variables only. For $x-x_2<x_o-x_2$ and $L=2\mu^{-1}\varepsilon\delta^{-2}a_\infty^{-1}da_\infty/dy$:

$$dv_p/dx=\mu^{-1}\varepsilon dU/dy\, dU/dx \qquad (12)$$
$$Y = -2\,\mu^{-1}\varepsilon\,\delta^{-1}\mathrm{cosech}(\delta\zeta/2)\,(d\zeta/dy) \qquad (13)$$
$$\begin{aligned}v_p = &[1-G(x,y)^2]^{-1}\{Y-L\,K\,(x-x_2)\}+\\ &+L\ln[(1+G(x,y))/(1-G(x,y))]\tanh(\delta\zeta/4)^{-1}\end{aligned} \qquad (14)$$

See that a_i and a_∞ vary in finite gaps due to dissociation changes that overcome migration of non-reacting ions. For 2D cases with a fixed wall potential U_w, ϕ_w≡U_w-U is the total EBL cross potential, at $\phi_w=0$, $d\phi_w/dy=(x_2K+1)\,d\zeta/dy$, so for linear U profile outside a PB EBL,with K and capacitance definitions, it is possible to write:

$$\begin{aligned}&d\phi_w/dy=-0.5(U_w-\zeta)a_\infty^{-1}da_\infty/dy\\ &-0.5\delta U_w[\tanh(\delta\zeta/2)]^{-1}d\zeta/dy+\\ &+0.5\delta\zeta\tanh(\delta\zeta/2)d\zeta/dy\end{aligned} \qquad (15)$$

The integral of $\gamma_e(u_p+u_m+v_p+v_{OHP})$ in the $\hat{\mathbf{e}}_x\hat{\mathbf{e}}_z$ planes is the flow current. As dEBL is thicker for low ϕ_w the peak u_p+v_p is in low ϕ_w zone, where flow current is minimal. Ignoring EBL area in mass balance $U_m(y)=\ddot{U}_m-\Sigma\{v_{p\infty}(y)+u_{p\infty}(y)+v_{OHP\infty}(y)\}/2$, and integrating 2nd line of equation (11) for given tube end pressures, one gets $\ddot{U}_m$. For tubes of 10^{-5} m, U profile is near linear, to 10^{-8} m systems, flow current is high and this ionic potential drop outside EBL is nonlinear, so iterative schemes and $\hat{\mathbf{e}}_y$ interpolation are used to find dU/dy. Equation (7) is solved only inside EBL, and out of it real profile approximated with straight line segments, as for each grid element current is assumed constant. v_{OHP} minimizes the sum of plastic all dissipations, including the nEBL plastic one if ϕ_w is high. For EBL thickness with small face grid scales, it is wise to supply the total EBL slip to the CFD model as a function of local ϕ_w. In general electrode potentials, total current and chemical kinetic models the are known. EKF test set ups have one channel and connected metal surfaces in short circuit, so the ϕ_w profiles minimize capacitive energy. Reactions may occur in insulated metallic parts, as tips work either as a secondary cathode or anode if $d\phi_w/dy$ is high. For **n** molecules by unit of volume with mean cross section diameter ξ, the mean free path λ is $(2^{0,5}\pi\, n\,\xi)^{-1}$.

Reference [20] hints a slip $(2-\alpha)\mu^{-1}\alpha^{-1}\lambda\tau_x+75(\gamma-1)\gamma^{-1}\mu\omega^{-1}T^{-1}dT/dx$. Its dT/dx part ($\psi$) is the thermocapillary slip, τ_x is the hydrodynamic stress $\mu du_m/dx$, α and γ accommodation coefficients. For high ϕ_w, x_o-x_2 and ζ vanish. Using this hint $v_{OHP}=(2-\alpha)\mu^{-1}\alpha^{-1}[\mu\lambda du/dx+\mathbf{h}\varepsilon c\phi_w E_o]$, with $\mathbf{h}=0$ for $\phi_w<\phi_c$, the potential the nEBL reaches yield strength. EBL forces bias the molecules shifts due to thermal shocks. Thus, it may happen that always $\mathbf{h}\neq 0$, v_p and u_p may be high in some points, but cathodic and anodic values are opposed to each other, and don't explain EKF for asymmetric ϕ_w fields. Equation (14) is not true at $\phi_w=0$, where a wall outward wall flow can´t be ignored, $s\neq 0$. v_p and v_{OHP} main driver is the electrostatic pressure change, due to charge unbalances in EBL. Without dEBL, it is easy to see that the nEBL pressure gradient times its thickness is exactly the electrocapillary force. This equality is always true, although it is not so easy to prove. Multiplying ψ by $u\omega d\mu^{-1}$, it is easy to see that ψ is a speed. It is interesting to see that at high boundary layer transverse potential, diffuse sublayer vanishes, a condition where electrocapillary forces are more important, so non-diffuse boundary layer shall move to reduce dissipation in this case.

The total tubes area A is easily found with its volume fraction f, external diameter d and layer thickness ♦ as $A=4f$♦d^{-1}. Similarly any nm-texture catalyst support area per unit of volume is proportional to the inverse of a characteristic dimension. Local electrode overpotential $\eta=RT\ln\{j^2[a_o]^{-2}4FD_{eff}i_o\kappa\}/(nF\alpha)$, with α accommodation coefficient, n the total number of charges moles involved, i_o the exchange current, D_{eff} the effective diffusion coefficient, $[a_o]$ the reference activity, j the ionic current density (A/m^2) and for systems without EKF, ionic losses obey:

$$d^2\eta/dy^2=-\Lambda\exp(0.5\alpha\eta n_1FR^{-1}T^{-1})= \\ =-\Lambda\exp(\eta\theta) \tag{16}$$

where Λ is $2r_{eff}^{-2}\rho[a_o]\{2D_{eff}nFri_o[a]\}^{1/2}$, n_1 is the number of moles of electron exchanged in the step or reaction mechanism, r the real radius and r_{eff} an effective radius, and ρ the ionic resistivity. As the right side of (16) does not depends on y, by analogy $d\eta/dy$ is $\{2\Lambda\exp(\eta\theta)/\theta+K\}^{1/2}$ which is easily integrated with help of item 2.315 of [21]. The 2 involved constants are obtained with the no ionic current condition at the tube end and membrane current condition easily for carded tubes (all current are equal). For entangled fabrics, tubes are different, the sum of all current is new, and individual currents solved individually by iterative way with its relation to overpotential curves. For EKF case Galerkin method was used, and the program verified with some no flow cases to improve its reliability. It is important to say that ionic losses plus chemical ones are limited by the average chemical losses necessary to held the current with nominal catalyst area and constant polarization plus the ionic losses related to uniform reaction rates. Activity distribution solutions are exponential (plane geometry) or I_o Bessel functions.

4 Electrokinetic Experimental Issues

The theoretical model parameters were found with the setup showed in Figure 1. Electroplating tapes were placed to avoid unpredicted passages due to distortion of PVC parts. The potential difference cross the 2 pools gives passages ionic current. Applied current was measured directly. Both currents are equal if applied potential is less than twice the electrolysis one, if not metal channel metallic annexes work either as a secondary anode or cathode. Ionic resistivity ρ was found with fixed current, i, and 2 smooth gold plates of area S in a rectangular box. Moving a plate, only the current path L changes, so the steady state applied potential change is $i\,\rho\Delta L/S$. The rest of applied potential is due to activation and boundary layer polarizations (see figure 2). All parts were jointly electroplated, with distinct cathode current controls. Due to some degree of porosity and corrosion, it was not possible to do alkaline tests, or to replace the tape barrier by more regular one.

Figure 1: EKF test arrangement

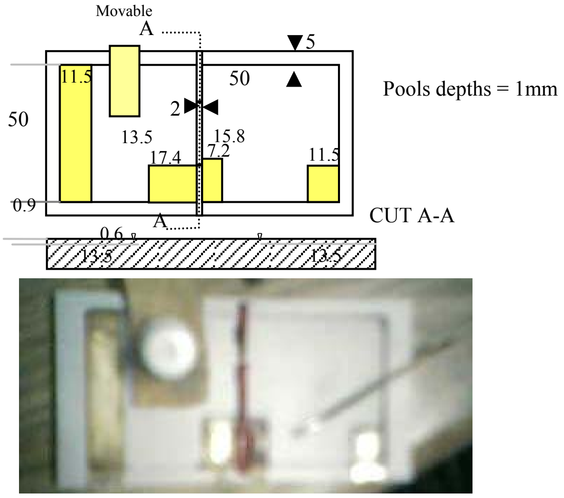

Figure 2: Ionic Conductivity Test Setup

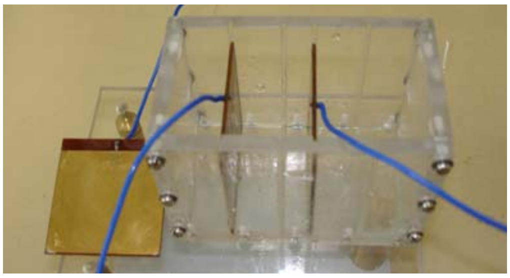

Acid tests were filmed with applied potential at main electrodes from 1.4 to 3.0 V, in 0.2 V steps. Bubbles hit one another in the channel to form bigger bubbles, and vanish as they reach the fluid upper surface, or a wall. All 63 s films showed 3 to 5 bubbles that pass directly through the entire channel. Events were observed frame by frame with the VirtualDub software, to obtain the mean bubble speed in the channel to each applied potential. Selected frames were exported to JPEG format with this tool. Figure 3 shows 5 frames from one of the films that shows a bubble passing the channel. Mean speeds are proportional to mean surface tension force. The capacitive energy of metal channel system is minimal, so the anodic zone has a limit capacitance of 0.2 F/m^2, and 0.7 F/m^2 in cathodic zone, and channel tip potentials were found to be at a rate of 0.37 in modulus.

Figure 3: Bubble flow in a very clean metallic channel

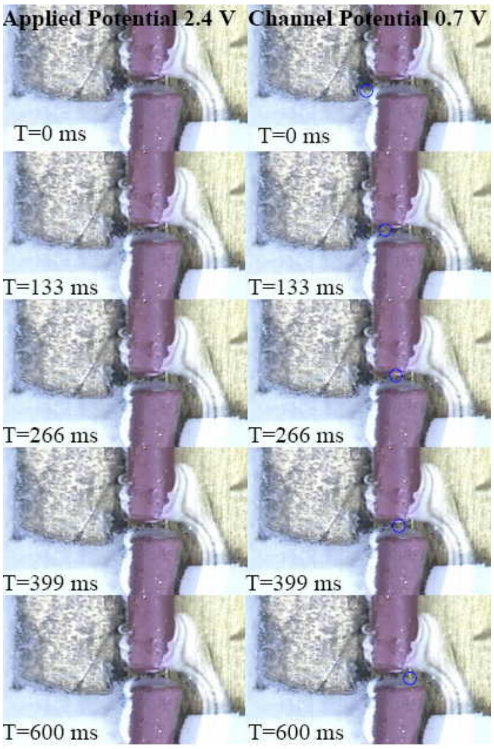

Table 1: Test Data Summary for H_2SO_4 6 M solution.

Total Potential (V)	**Channel Potential** (mV)	**Current** (mA)
1.40	166	1.15±0.15
1.60	371	3.5±0.3
1.80	563	12.5±0.3
2.00	754	18.4±0.3
2.20	959	22.3±0.3
2.40	1.21	29.3±0.2
2.60	1.32	36.7±0.3
2.80	1.57	42.3±0.1
3.00	1.76	50.0±0.1

Total channel potential were measured with Pt 36 AWG wires. With this **h** was found to be 57±15. Errors come from corrosion rate, oxidation, bad cleaning, and electrical measurements errors, as nEBL thickness of clean surfaces are below 0.3 nm. Cleaning is decisive to EKF intensity level.

5 Cell Performance Analyses

Nano-structured porous µ-tube fuel cells, see figures 4 and 5, are studied in this section. Nickel nm-foam wall protected by a layer of Ni-Cr nitride may be operated in acid media with this cover, but it was initially planed to operate with alkaline electrolytes. Figures 10-12 give theoretical results for: output potential, efficiency and power for each current without[a] or with[b] EKF. These data do not consider air channels, that have equal width entrances at opposite electrode sides, and end with null width. CFD analysis points air channels using 22- 40% of cell cross section. Bipolar plate and insulator are 60 µm thick, allowing 8.9-12.2 electrodes pairs/cm. The spinel catalyst exchange current the was $3{\cdot}10^{-5}$ A/m^2. 35% of foam volume are carded tubes of 5/7 µm inner/outer radius, 100 nm foam cells with 85% void. Pt O_2 exchange current is 0.07 A/m^2. CFD analysis, with OpenFoam and CFX, predicted 6 to 9 Bénard cells for 0.4 mm long carded set ups with fibers normal to ionic insulation. Strong wall outflows near the ionic zero cause such cells, with 30-150 µm lengths. It shall be seen that even without EKF, theoretical performances of proposed cells are promising.

Figure 4: Metal (Ni) nm-foam wall m-tubes AFC

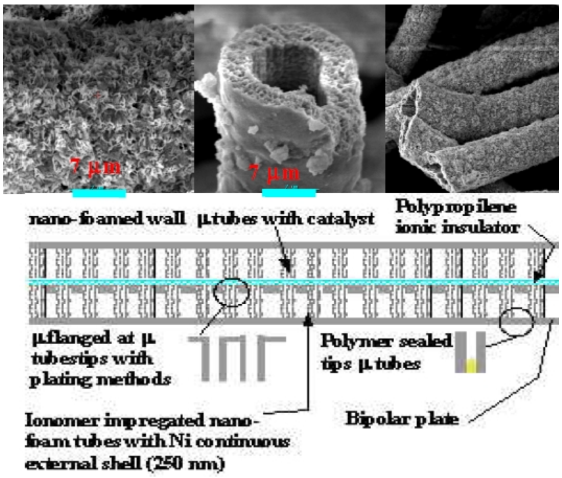

Cell performance curves were based on chemical kinetic models and on energy conservation, so output voltages are the c Pt ¨ less the integral of all losses, divided by the cu catalyst $)_2$ and H_2 local levels, catalyst data and diffusion flux limits were used to calculate local reaction rates and output currents. Overpotential losses are less relevant in high breathing area systems, as the proposed one, than planar systems. The systems does not have electrodes of high electrical resistance due to contact resistances. The ionic resistance of the electrical insulator is much smaller than any membrane one. A cell of porous carbon tubes with gas inside, catalyst and Nafion outer coats, with tubes in an electrolyte pool, has power over 8 W/cm^3 [14], despite of its tubes separation, confirming the importance of better breathing.

Figure 5: Entangled Carbon nm-tubes wall μ-tubes cell.

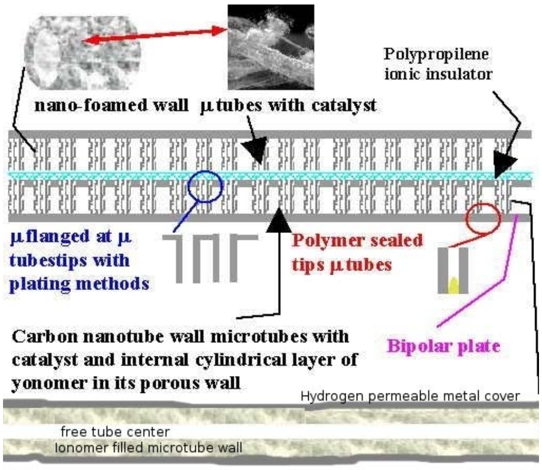

Figure 6: Nickel nm-foam cell alkaline performance

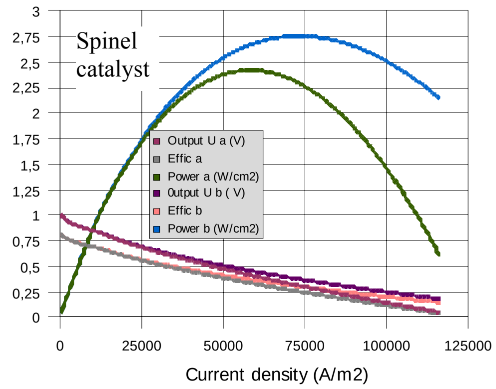

Figure 7: Nickel nm-foam tubular acid performance

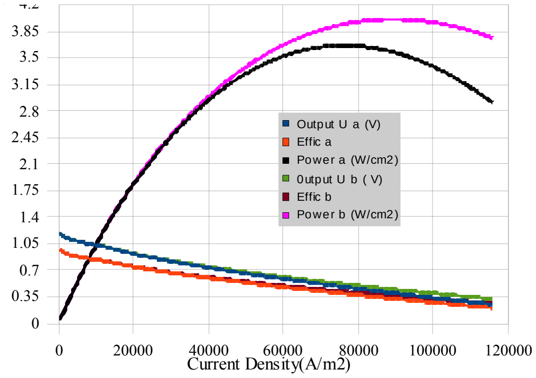

Figure 8: Entangled nm-tube wall cell performance.

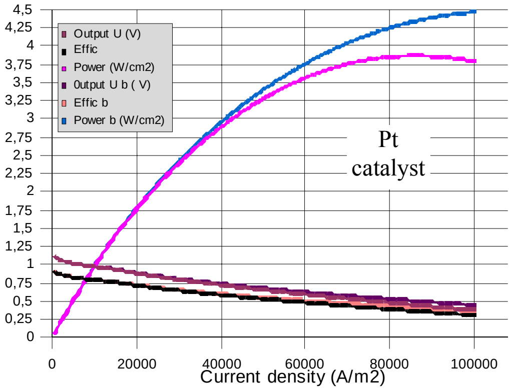

Theoretical results for flow current in non-reacting Ni m-tubes with nm-foam walls are in table 2. Table 3 gives complete fuel cell performance considering gas passages and reduction of electrode area. The gas flow limits either reduction of electrode thickness of further reduction in fiber diameter, and for carbon electrodes. Anodes partially filled with ionomer may have alcohol external catalyst, and be thiner than hydrogen anodes.

Table 2: Flow current data for Ni μ-tubes cell with 6 M KOH.

Applied Potential (V)	**Total Lenght** (mm)	**Null ϕ_w Point** (mm)	**Peak Flow Current** (μA)	**Meam Bulk Current** (μA)
0.1	0.80	0.10	0.0487	0.0188
0.2	0.80	0.10	0.383	0.0377
0.3	0.80	0.10	1.29	0.0565
0.4	0.80	0.10	3.07	0.0754
0.1	0.80	0.40	0.0335*	0.0188
0.2	0.80	0.40	0.224	0.0377
0.3	0.80	0.40	0.755	0.0565
0.4	0.80	0.40	1.79	0.0754

Table 3: Complete Fuel Cell Performances Considering gas passages

Cell tube wall & media	gas flow area (%)	Peak power (W/cm^2)		Peak power (W/cm^3)		Associated current (A/cm^2)	
Ni KOH	25	1.82	2.07	16.2	18.4	4.38	5.49
Ni-Cr-N acid	25	2.76	3.02	24.6	26.9	5.75	6.83
Carbon acid	35	2.51	2.93	30.6	36.1	5.59	6.96

6 Conclusions

The μ-tubular arrangements allows gas liquid interface areas over 50 times bigger than bipolar separators nominal cross section. This together with flow current due to electrokinetic effects, that reduces ionic current losses in clean electrodes to 50% of unclean electrodes values and enable these arrangements to deliver over 24 W/cm^3 at near 50% efficiency if clean, a power at least 12% over unclean output one. Better O_2 transport, thanks to higher gas-liquid interface areas, is the major cause of better performance. High gas liquid interfaces dismiss the need of very effective catalysts. The joint use of better geometries and new catalysts will enable low cost fuel cells to deliver 13 to 32 W/cm^3 with efficiencies over 50% in about a decade, with great impacts on the energy market. Anode hidden catalyst is a concept that protects it from poisoning due to a 10 to 35 nm compact nickel shell, or thicker Nb or V metal ones plated with low temperature ionic liquids. The preliminary tests of manufacturing process of proposed cells geometry showed good results, and may lead to a complete cell with proper financing in one or two years.

References

[1] Antoine, O; Bultel, Y; Durand, R. "Oxygen reduction reaction kinetics and mechanism on platinum nano-particles inside Nafion". *Journal of Electroanalytical Chemistry* 499, 2001, pp. 85–94.

[2] Easton, E.D. "Chemical Modification of Fuel Cell Catalysts and Electrochemistry of Proton Exchange Membrane Fuel Cell Electrodes", PhD Thesis. University of Newfoundland. Canada. 2003.

[3] Tromans, D. "Oxygen Solubility Modeling in Aqueous Solutions". 0-7803-5489-3/99/$10.00 01999 IEEE

[4] Mitchel, W. "Fuel Cells". Academic Press. 1963.

[5] Ledoux, M.J; Vieira, R; Pham-Huu, C; Keller, N. "New catalytic phenomena on nano-structured (fibers and tubes) catalysts". *Journal of Catalysis* 216, 2003, pp. 333-342.

[6] Bambace, L.A.W; Nishimori, M; Ramos, F. M, Melo, C.J; Kuranaga, C; Senna, J.R.S; Neri, J.A.C.F; Silva, M.D. "Conjunto capilar recirculante para células a combustível". Brazilian Patent Pending PI0301417-7. May. 2003.

[7] Bambace, L.A.W; Ramos, F.M; Melo, C.J; Nishimori, M; Kuranaga, C. "Sistema de tubos de parede eletrodepositada para células a combustível". Brazilian Patent Pending PI0301416-9. May,. 2003.

[8] Bambace, L.A.W; Castro, A.J.A; Ramos, F.M; Nishimori, M; Favali, R.C. "Ânodo para Célula a Combustível Baseado em Microtubos com Paredes Porosas Nanoestruturadas Impregnadas". Brazilian Patent Pending. Aug. 2007.

[9] Bambace, L.A.W; Castro, A.J.A; Ramos, F.M; Nishimori, M; Favali, R.C. "Ânodo para Células a Combustível Baseado em Microtubos com Paredes Porosas Nanoestruturadas a Base de Carbono Parcialmente Impregnadas de Ionômero". Brazilian Patent Pending. Sept. 2007.

[10] Bambace, L.A.W; Castro, A.J.A; Ramos, F.M; Nishimori, M; Favali, R.C. "Cátodo para Células a Combustível de Microtubos de Paredes Porosas de Níquel Nanoestruturadas Ativadas com Catalisador". Brazilian Patent Pending. Aug. 2007.

[11] Bambace, L.A.W; Castro, A.J.A; Ramos, F.M; Nishimori, M; Favali, R.C. "Eletrodo para Células a Combustível Baseado em Microtubos de Paredes Nanoestruturadas de Material Carbonetado e Catalisador de Espuma Metálica Nanoestruturada". Brazilian Patent Pending. Aug. 2007.

[12] Bambace, L.A.W; Castro, A.J.A; Ramos, F.M; Nishimori, M; Favali, R.C. "Cátodo para Células a Combustível de Microtubos de Paredes Porosas de Emaranhado de Nanotubos de Prata". Brazilian Patent Pending. Aug. 2007.

[13] Bambace, L.A.W; Nishimori, M; Ramos, F. M.; Bastos-Netto, D. "Performance of a double catalyst fuel cell cathode with a tubular oxygen breathing and preliminary reduction zone". Journal of Thermal Science 14(2). 2005. pp. 187-192.

[14] Tennison, S.R; Strelko, V; Brown, D.E; Sowerby, B. "Novel high power density carbon fibre based PEM fuel cells - Feasibility Study" MAST Carbon Ltd Report ETSU F/02/00247/00/REP. 2003

[15] Bazylak, A; Sinton, D; Djilali,N. "Improved fuel utilization in microfluidic fuel cells: A computational study". Journal of Power Sources 143, 2005, pp. 57-66.

[16] Min, K; Tanaka, S; Esashi, M. "Fabrication of novel MEMS-based polymer electrolyte fuel cell architectures with catalytic electrodes supported on porous SiO2". J. Micromech. Microeng. 16, 2006, pp. 505–511.

[17] La Coura, B.R;Schieveb, W.C. "Derivation of the Onsager principle from large deviation theory" Physica A 331, 2004, pp. 109 -124.

[18] Vine, S; Outhwaite, C.W. "Comparison of Theories of the Aqueous Electric Double Layer at a Charged Plane Interface". Biophysical Journal 84, 2003, pp 3594–3606.

[19] Corry, B; Kuyucak, S; Chungy, S. "Dielectric Self-Energy in Poisson-Boltzmann and Poisson-Nernst-Planck Models of Ion Channels". J.C.S.Faraday II, 74, 1978, pp 1670-1689.

[20] Dadzie, S.K; Méolans, J. G. "Temperature jump and slip velocity calculations from an anisotropic scattering kernel". Physica A 358, 2005, pp. 328-346.

[21] Gradshteyn, I.S; Ryzhik, I.M. Table of Integral, Series and Products. Academic Press. NY. 1965.